Measurement report: Impact of domestic heating on dust deposition sources in hyper-arid Qaidam Basin, northern Qinghai-Xizang Plateau

Haixia Zhu[abc], Lufei Zhen[abc], Suping Zhao[d]*, Xiying Zhang[ab]*

[a] Key Laboratory of Green and High-end Utilization of Salt Lake Resources, Qinghai Institute of Salt Lakes, Chinese Academy of Sciences, Xining, 810008, China.

[b] Qinghai Provincial Key Laboratory of Geology and Environment of Salt Lakes, Qinghai Institute of Salt Lakes, Chinese Academy of Sciences, Xining, 810008, China.

[c] University of the Chinese Academy of Sciences, Beijing, 100049, China

[d] Key Laboratory of Cryospheric Science and Frozen Soil Engineering, Northwest Institute of Eco-Environment and Resources, Chinese Academy of Sciences, Lanzhou, 730000, China

*_Correspondence to:_ Xiying Zhang (xyzhchina@isl.ac.cn) and Suping Zhao (zhaosp@lzb.ac.cn)

26 pages of Supporting Information

I. Page S2-S4, Supporting Text

II. Page S5-S9, Supporting Tables (Table S1-S3)

III. Page S10-S26, Supporting Figures (Figures S1-S13)

Supporting Text

PMF Source apportionment initialization

The source apportionment of dust deposition utilized the EPA PMF 5.0 model to analyze 109 samples based on their respective sampling sites. Internal PMF parameters, such as Q_{robust}, Q_{true}, and $Q_{expected}$ were considered to assess performance of PMF. In general, Q is a measure of the fitness of the model; Q_{robust} is calculated using only samples that fit the model well, while all samples are used in calculating Q_{true}. $Q_{expected}$ is equal to the number of samples multiplied by the number of strong species. Multiple iterations of each dataset were processed to identify consistent Q values. Testing for factor peak values across 3 to 6 factors revealed that 4 factors provided the best solution for XZH, LTC, and BLX, while 5 factors were optimal for GEM, NMH, and DLX (Figure S14). High determination coefficients (R^2 = 0.64~0.98) indicated a strong correlation between calculated and measured element fluxes, with intercepts and slopes nearing unity. The analysis found no need for factor rotation, and the Q_{robust} values closely aligned with the Q_{true}, suggesting a good model fit. Bootstrapping was not used because of the small size of the sample set. High uncertainties were observed in the contribution of certain species to each factor, but each factor contained at least one well-constrained species, highlighting the dominant chemical characteristic of that factor. These high uncertainties stem, in part, from the high and variable values of field blanks that are carried through the model. Rotational swaps, indicating uncertainty in the identified components and their contributions, were not observed during displacement, and the largest change in Q was -0.01%, evidencing the good fit of the solution set.

A theoretical Q-value (also referred to Q_{exp}) may be approximated as a number of points in the data matrix minus the total number of elements in the factor matrices (Paatero and Tapper, 1994)

$$Q_{exp} = n \cdot m - N \cdot (n + m), \quad (1)$$

where n is the number of samples, m is the number of species and N is the number of obtained factors. Large deviation from the Q_{exp} may indicate that a larger extra modeling uncertainty is needed. The optimal number of factors was determined based on the variation in the Q_{robust}/Q_{exp} ratio and the interpretability of the analytical factor distribution. In our study, the Q_{true}/Q_{robust} ratios for the PMF models at all six monitoring stations were below 1.5, indicating that the simulation results are reasonable. Additionally, the Q_{robust}/Q_{exp} ratio confirms that our simulated results align

with the optimal number of factors.

Error estimates of the base PMF solution are provided through combination of Displacement (DISP) and Bootstrap (BS) tests (DISP-BS). Displacement test explores the rotational ambiguity of the solution by assessing the largest range of source profiles without significant increase in the Q value. DISP%dQ is the parameter displaying in the displacement result matrix. If DISP%dQ is equal to zero that means the displacement analysis result is considered as acceptable. The displacement swap counts (DISP swaps) are a key indicator of the stability of a PMF solution. If it swaps it indicates that there is significant rotational ambiguity and that the solution is not sufficiently robust to be used. Error estimates of the base solution are provided through combination of both Displacement (DISP), and Bootstrap (BS) tests (DISP-BS) (Manousakas et al., 2017).

BS detects disproportionate effects of a small set of observations on the solution and also, to a lesser extent, effects of rotational ambiguity. Mapping of bootstrap factors to base factors is a summary result on factors mapping. Ideally BS factor mapping should be one-to-one with respect to base run factors. Nevertheless, factors with more than 80% mapping are considered acceptable. Base random seed is the seed number corresponding to the result with minimum Q and allows reproducing the same results of PMF solution.

In our study, the decline in DISP%dQ remained consistently within 0.1%, indicating that the global minima of dQ were achieved under the tested configurations. Throughout the four dQmax levels, no factor switching occurred during the DISP run phase, and the factor matching rate during the BS phase exceeded 85%. Additionally, there was no factor switching in the BS-DISP run phase. These findings underscore the stability of the PMF model results (Paatero et al., 2014; Brown et al., 2015; Li, 2020).

Reference

Brown, S.G., Eberly, S., Paatero, P. and Norris, G.A. (2015) Methods for estimating uncertainty in PMF solutions: examples with ambient air and water quality data and guidance on reporting PMF results. Science of the Total Environment 518-519, 626-635.

Li, J., Teng, Wu, J., Chen, H., and Jiang, J. (2020) Uncertainty in identifying soil heavy metal sources using the PMF model (in Chinese). China Environmental Science 40(2), 716-725.

Manousakas, M., Papaefthymiou, H., Diapouli, E., Migliori, A., Karydas, A., Bogdanovic-Radovic, I. and Eleftheriadis, K. (2017) Assessment of PM2. 5 sources and their corresponding level of uncertainty in a coastal urban area using EPA PMF 5.0 enhanced diagnostics. Science of the Total Environment 574, 155-164.

Paatero, P., Eberly, S., Brown, S.G. and Norris, G.A. (2014) Methods for estimating uncertainty in factor analytic solutions. Atmospheric Measurement Techniques 7(3), 781-797.

Paatero, P. and Tapper, U. (1994) Positive matrix factorization: A non-negative factor model with optimal utilization of error estimates of data values. Environmetrics 5(2), 111-126.

Supporting Tables

Stations	Latitude (°)	Longitude (°)	Description
XZH	93.67964745	36.79841344	*Lycium* berry cultivation base, national climate benchmark station
GEM	94.90930080	36.42121338	The largest city in the Qaidam Basin, with a high population
LTC	95.77349782	36.49093842	Desert with camel breeding farms
NMH	96.42957687	36.44058390	Towns with extensive *Lycium* berry cultivation in the surrounding areas
BLX	97.53657818	36.16438395	Pasture with developed agricultural practices
DLX	98.09684336	36.29662699	County seat with a relatively large population and a thriving mining industry

Table S1 Geographic coordinates and descriptions of monitoring stations in the study area. The table lists the latitude and longitude of each site, along with a brief description of the local characteristics and land use. [XZH, Xiao Zaohuo station; GEM, Golmud station; LTC, Da Gele station; NMH, Nuo Muhong station; BLX, Balong station; DLX, Dulan station].

	Rural-HP	Rural-NHP	Urban-HP	Urban-NHP
Q_{exp}	160	157	111	195
Q_{robust}	908.43	813.39	462.26	1429.10
Q_{true}	1131.91	1095.23	463.26	1811.90
Q_{true}/Q_{robust}	1.25	1.35	1.00	1.27
Q_{robust}/Q_{exp}	5.68	5.18	4.16	7.33
Converged	Yes	Yes	Yes	Yes
DISP % *dQ*	<0.1%	<0.1%	<0.1%	<0.1%
DISP % swaps	0%	0%	0%	0%
BS R^2	0.6	0.6	0.6	0.6
BS mapping	93%	94%	89%	88%
BS-DISP %swaps	0%	0%	0%	0%
Extra modeling uncertainty	0%	0%	0%	0%

Table S2 Summary of PMF and error estimate diagnostics

City	Country	Element					Reference
		Cd	Cr	Cu	Pb	Zn	
Guangzhou	China	1.00-7.44	28.3-121	52.7-261	39.2-123	245-1007	Cai et al., 2013
Xi'an	China	4.18±1.20	195.92±48.66	125.31±78.80	310.29±80.79	721.20±237.57	Chen et al., 2017
Suzhou	China	0.25-26.9	11.9-110	13.2-1200	30.5-2240	47.6-4290	Ma et al., 2016
Changsha	China	9.11	80.7	43.9	66.6	215	Li et al., 2016
Beijing	China	0.130-5.01	32.0-227	5.46-623	16.7-2450	57.4-908	Wei et al., 2015
Tianjin	China	0.22-1.38	30.9-225	20.7-188	20.6-156	–	Yu et al., 2014
Huainan	China	0.110-0.449	40.5-129	19.1-87.5	21.2-71.5	–	Tang et al., 2017
Shanghai	China	0.36-4.72	18.0-1325	17.0-1175	28.0-4443	82-2140	Shi et al., 2008
Urumqi	China	0.44-2.40	24.85-102.67	27.13-105.54	4.56-63.46	208.65-2375.97	Wei et al., 2015
Lanzhou	China	0.102-3.21	18.8-135	33.6-151	8.42-61.0	41.5-109	Jiang et al., 2018
Jinan		0.90-3.96	35.17-3126.00	27.15-156.60	46.14-235.20	115-1645	Pang et al., 2014
Galicia	Spain	0.08-0.89	35.4-82.92	5.8-58.7	0.87-271.9	30.7-543.3	Franco-Uria et al., 2009
Alexandria	Egypt	0.33	24.3	79.7	70.3	169	Dat et al., 2021
Ho Chi Minh City,	Vietnam	0.5	102.4	153.7	49.6	466.4	Jadoon et al., 2021
Cantabria region	Spain	0.1	5.2	11.8	4.5	183	Fernandez-Olmo et al., 2015
Junggar Basin	China	16.65	605.5	100.1	–	5933.9	Yang et al., 2016
Ebinur Basin	China	0.004-0.48	58.15-169.25	15.12-62.27	11.14-124.17	26.25-227.51	Abuduwailil et al., 2015
	China	0.003-5.17	0.04-64.8	0-34.6	0-121.2	0.64-257.7	This study

Table S3 Comparison of dust-fall metal concentrations in this study with those from other regions

Reference

Abuduwailil, J., Zhaoyong, Z., Fengqing, J. (2015) Evaluation of the pollution and human health risks posed by heavy metals in the atmospheric dust in Ebinur Basin in Northwest China. Environmental Science and Pollution Research 22, 14018-14031.

Brown, S.G., Eberly, S., Paatero, P., Norris, G.A. (2015) Methods for estimating uncertainty in PMF solutions: examples with ambient air and water quality data and guidance on reporting PMF results. Sci Total Environ 518-519, 626-635.

Cai, Q.Y., Mo, C.H., Li, H.Q., Lu, H., Zeng, Q.Y., Li, Y.W., Wu, X.L. (2013) Heavy metal contamination of urban soils and dusts in Guangzhou, South China. Environ Monit Assess 185, 1095-1106.

Chen, Y., Zhao, J. J, Tang, D., Tian, X. L and Wu, Y.G. (2017) Characteristics of heavy metal pollution and ecological risk of atmospheric dust-fall in Xi'an (in Chinese). Arid Zone Resources and Environment 31, 154-159.

Dat, N.D., Nguyen, V.T., Vo, T.D., Bui, X.T., Bui, M.H., Nguyen, L.S.P., Nguyen, X.C., Tran, A.T., Nguyen, T.T., Ju, Y.R., Huynh, T.M., Nguyen, D.H., Bui, H.N., Lin, C. (2021) Contamination, source attribution, and potential health risks of heavy metals in street dust of a metropolitan area in Southern Vietnam. Environ Sci Pollut Res Int 28, 50405-50419.

Fernandez-Olmo, I., Puente, M., Irabien, A. (2015) A comparative study between the fluxes of trace elements in bulk atmospheric deposition at industrial, urban, traffic, and rural sites. Environ Sci Pollut Res Int 22, 13427-13441.

Franco-Uria, A., Lopez-Mateo, C., Roca, E., Fernandez-Marcos, M.L. (2009) Source identification of heavy metals in pastureland by multivariate analysis in NW Spain. J Hazard Mater 165, 1008-1015.

Jadoon, W.A., Abdel-Dayem, S., Saqib, Z., Takeda, K., Sakugawa, H., Hussain, M., Shah, G.M., Rehman, W., Syed, J.H. (2021) Heavy metals in urban dusts from Alexandria and Kafr El-Sheikh, Egypt: implications for human health. Environ Sci Pollut Res Int 28, 2007-2018.

Jiang, Y., Shi, L., Guang, A.L., Mu, Z., Zhan, H., Wu, Y. (2018) Contamination levels and human health risk assessment of toxic heavy metals in street dust in an industrial city in Northwest China. Environ Geochem Health 40, 2007-2020.

Li, F., Zhang, J., Huang, J., Huang, D., Yang, J., Song, Y., Zeng, G. (2016) Heavy metals in road dust from Xiandao District, Changsha City, China: characteristics, health risk assessment, and integrated

source identification. Environ Sci Pollut Res Int 23, 13100-13113.

Li, J., Teng, W. J., Chen, H. Y and Jiang, J. Y. (2020) Uncertainty in identifying sources of soil heavy metals using the PMF model (in Chinese). China Environmental Science 40, 716-725.

Ma, Z., Chen, K., Li, Z., Bi, J., Huang, L. (2015) Heavy metals in soils and road dusts in the mining areas of Western Suzhou, China: a preliminary identification of contaminated sites. Journal of Soils and Sediments 16, 204-214.

Paatero, P., Eberly, S., Brown, S.G., Norris, G.A. (2014) Methods for estimating uncertainty in factor analytic solutions. Atmospheric Measurement Techniques 7, 781-797.

Paatero, P., Tapper, U. (1994) Positive matrix factorization: A non-negative factor model with optimal utilization of error estimates of data values. Environmetrics 5, 111-126.

Pang, X. G., Wang, X. M., Dai, J. R., Guo, R. P., Yu, C., Cui, Y. J and Dong, J. (2014) Geochemical characteristics and pollutant end-member study of atmospheric dust-fall in Jinan (in Chinese). Chinese Geology 41, 285-293.

Shi, G., Chen, Z., Xu, S., Zhang, J., Wang, L., Bi, C., Teng, J. (2008) Potentially toxic metal contamination of urban soils and roadside dust in Shanghai, China. Environ Pollut 156, 251-260.

Tang, Z., Chai, M., Cheng, J., Jin, J., Yang, Y., Nie, Z., Huang, Q., Li, Y. (2017) Contamination and health risks of heavy metals in street dust from a coal-mining city in eastern China. Ecotoxicol Environ Saf 138, 83-91.

Wei, X., Gao, B., Wang, P., Zhou, H., Lu, J. (2015) Pollution characteristics and health risk assessment of heavy metals in street dusts from different functional areas in Beijing, China. Ecotoxicol Environ Saf 112, 186-192.

Yang, C., Tashpolat, T., Hou, Y.-J., Gao, Y.-X., Liu, F., Xia, N. (2016) Assessment of Heavy Metals Pollution and Its Health Risk of Atmospheric Dust Fall from East Part of Junggar Basin in Xinjiang (in Chinese). Environmental Science 37, 2453-2461.

Yu, B., Wang, Y., Zhou, Q. (2014) Human health risk assessment based on toxicity characteristic leaching procedure and simple bioaccessibility extraction test of toxic metals in urban street dust of Tianjin, China. PLoS One 9, e92459.

Supporting Figures

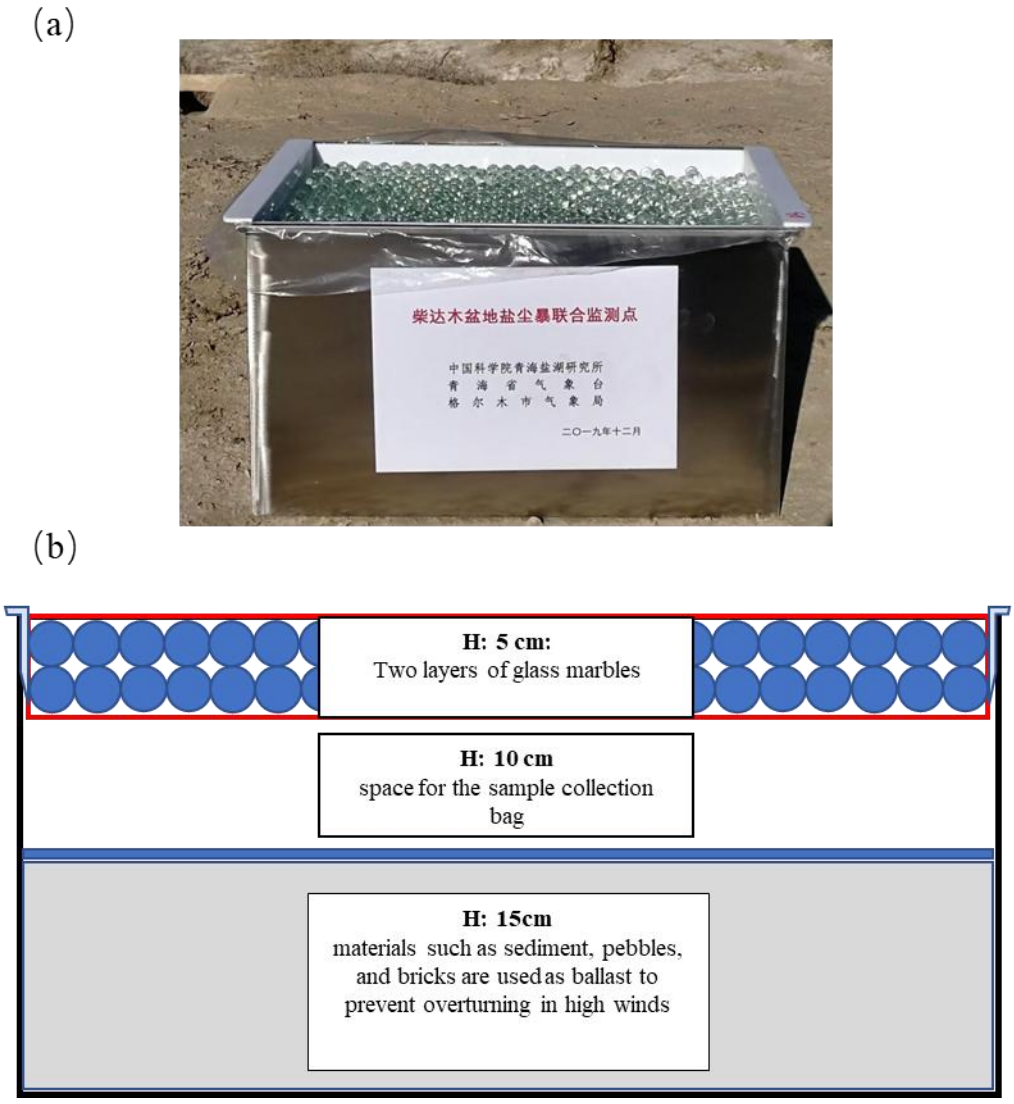

Figure S1. (a) Photo and (b) schematic of dust samples sampling device. The device is a stainless steel box measuring 50 cm in length, 30 cm in width, and 30 cm in height, consisting of three layers. The first layer, 5 cm deep, contains two layers of φ16 mm glass beads with a specific density. The second layer, 10 cm high, contains high-density polyethylene bags for dust collection. The third layer, 15 cm high, is constructed from sand pebble brick material to ensure equipment stability.

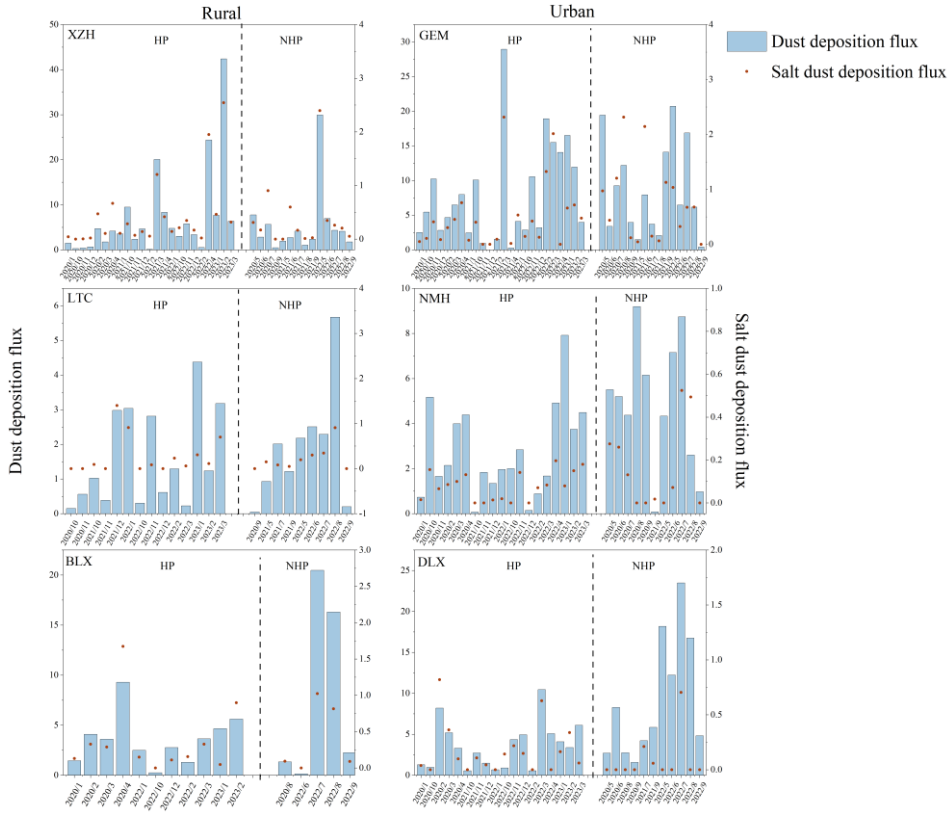

Figure S2 Temporal variation of atmospheric dust (DF) and salt dust deposition flux (SDF) at six stations during heating and non-heating periods. DF represented by blue bars and SDF by red circles. [HP, Heating period; NHP, Non-heating period; XZH, Xiao Zaohuo station; GEM, Golmud station; LTC, Da Gele station; NMH, Nuo Muhong station; BLX, Balong station; DLX, Dulan station]

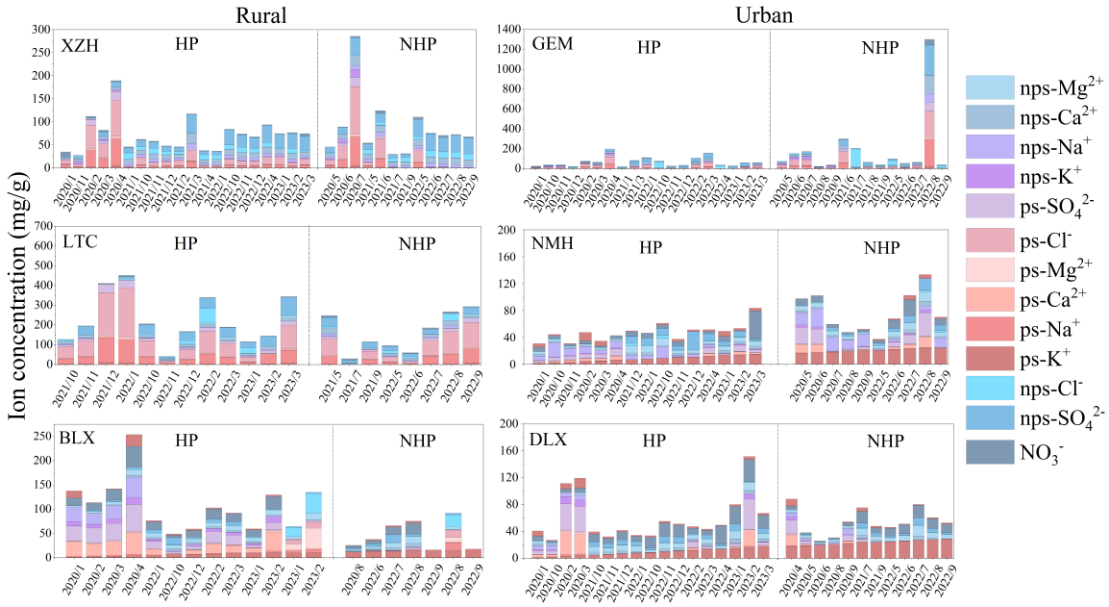

Figure S3 Temporal variations in ion concentrations at six monitoring sites during heating and non-heating periods. HP, Heating period; NHP, Non-heating period; XZH, Xiao Zaohuo station; GEM, Golmud station; LTC, Da Gele station; NMH, Nuo Muhong station; BLX, Balong station; DLX, Dulan station

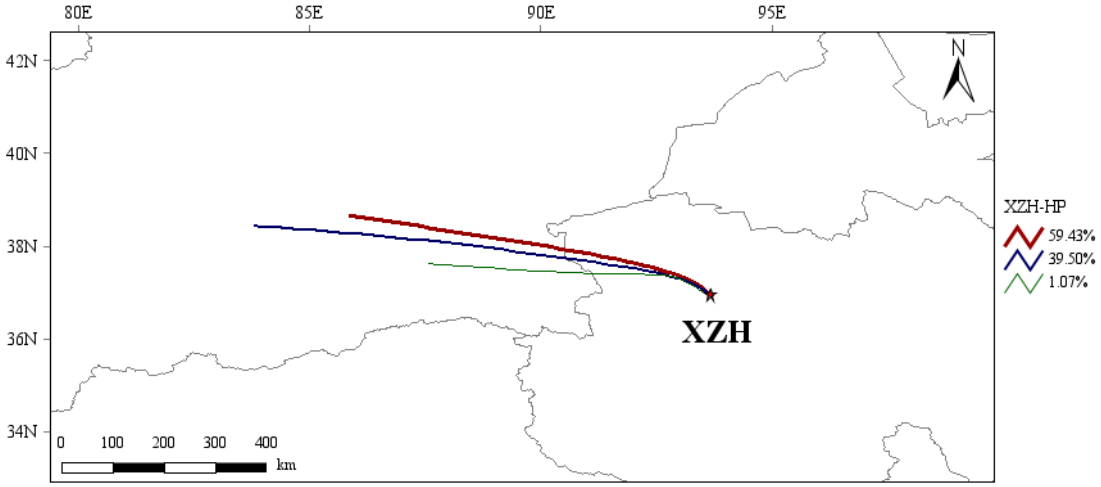
80E
85E
90E
95E
42N
40N
38N
36N
34N
N
XZH-HP
59.43%
39.50%
1.07%
XZH
0
100
200
300
400
km

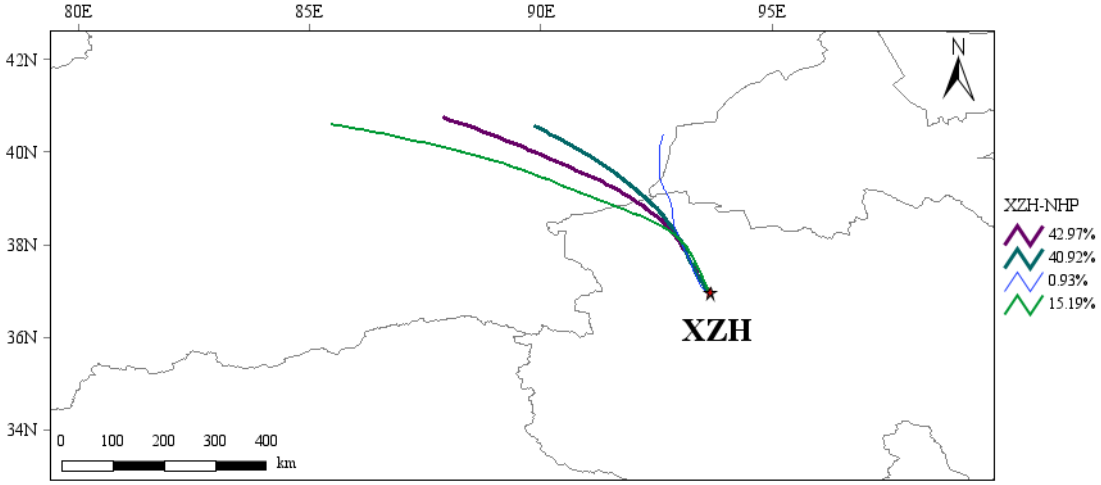
80E
85E
90E
95E
42N
40N
38N
36N
34N
N
XZH-NHP
42.97%
40.92%
0.93%
15.19%
XZH
0
100
200
300
400
km

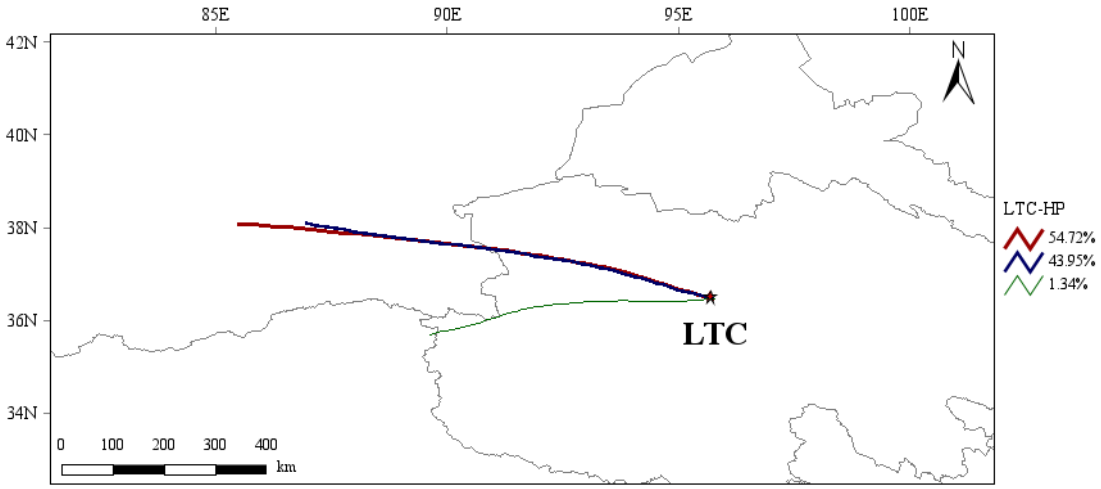
85E
90E
95E
100E
42N
40N
38N
36N
34N
N
LTC-HP
54.72%
43.95%
1.34%
LTC
0
100
200
300
400
km

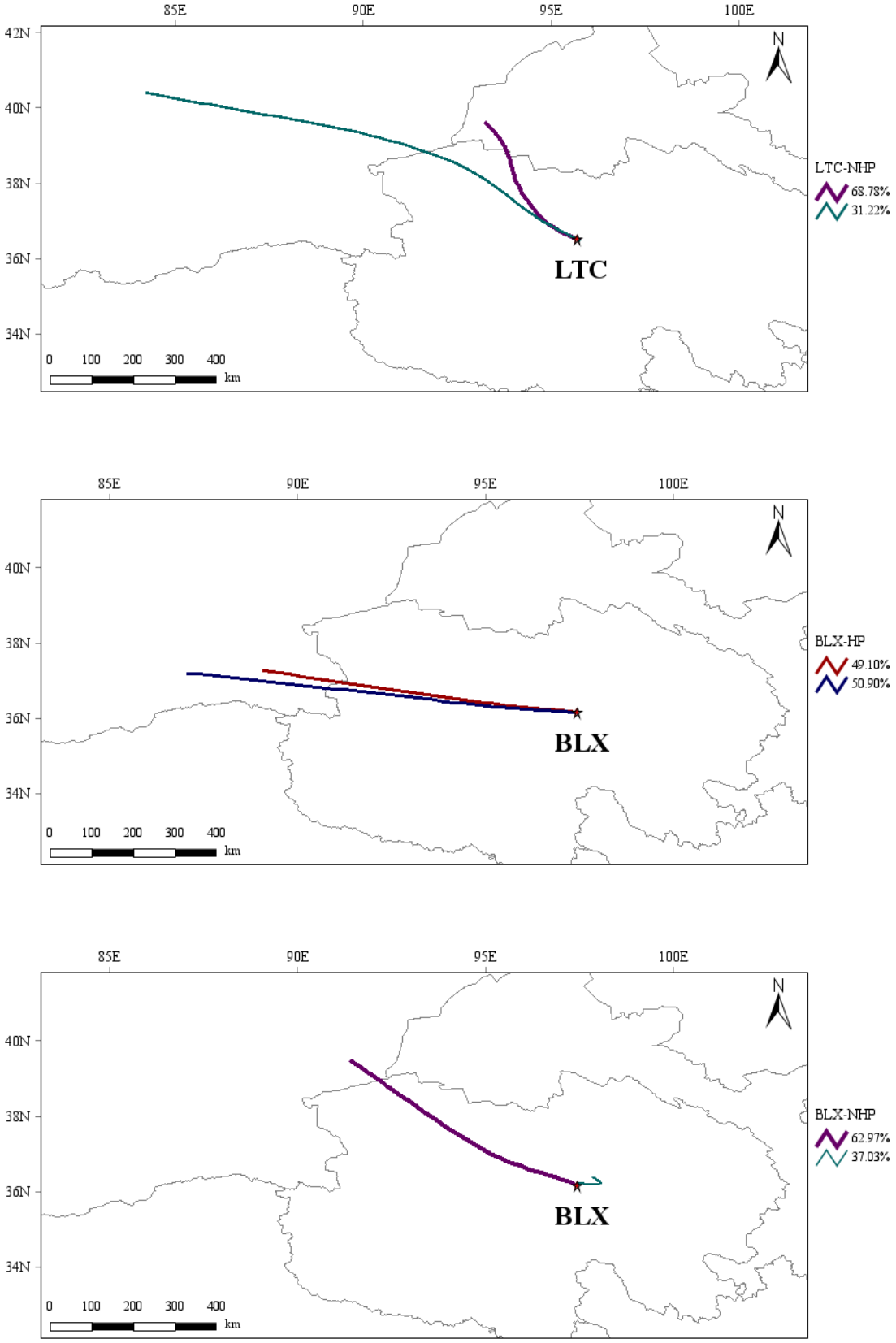

Figure S4 Backward trajectory simulations were conducted at rural monitoring stations during heating and non-heating periods. Different colors denote distinct trajectory paths, while

line thickness indicates the degree of contribution from each path. The red star marks the location of the stations. [HP, Heating period; NHP, Non-heating period; XZH, Xiao Zaohuo station; LTC, Da Gele station; BLX, Balong station].

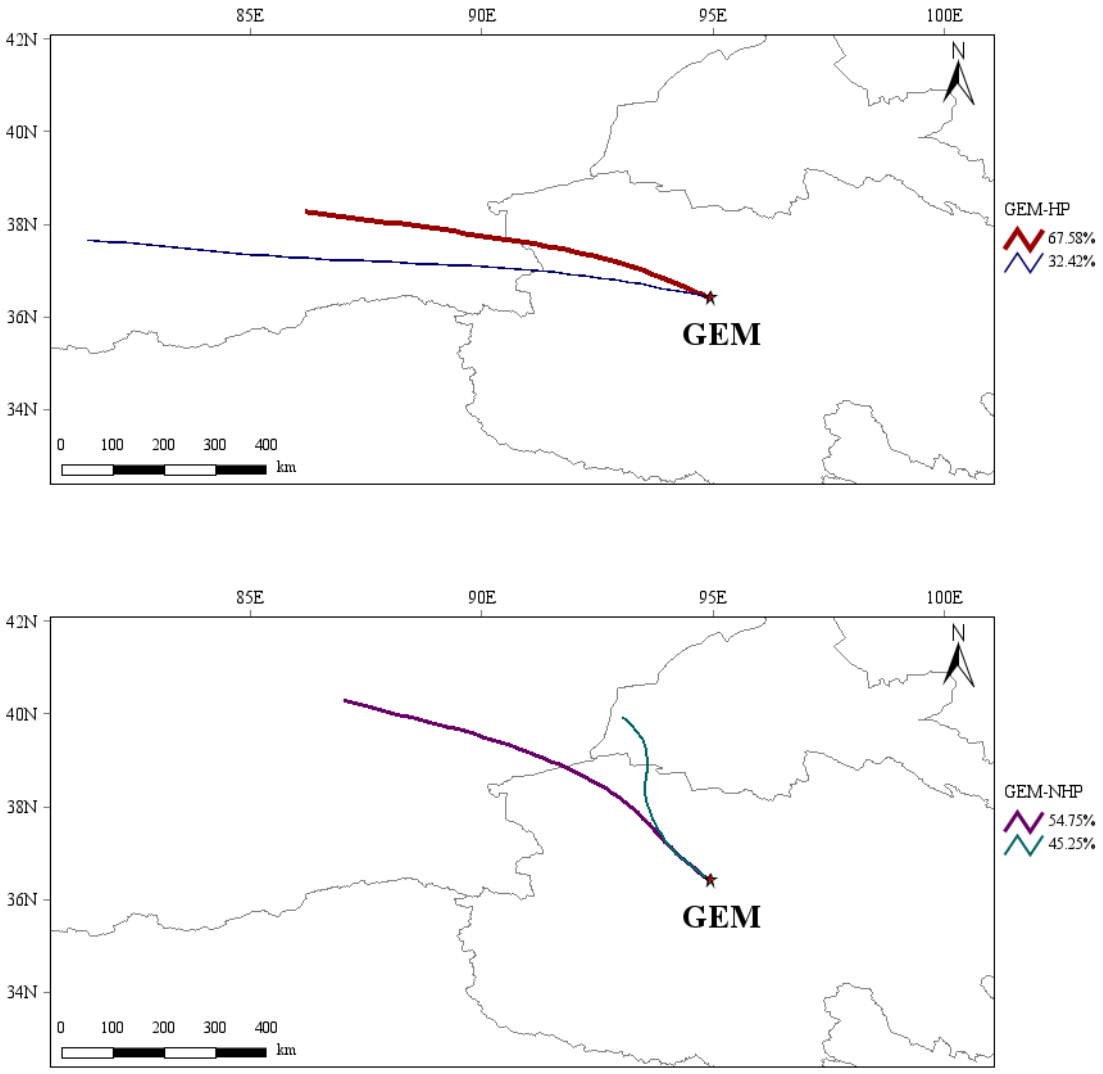

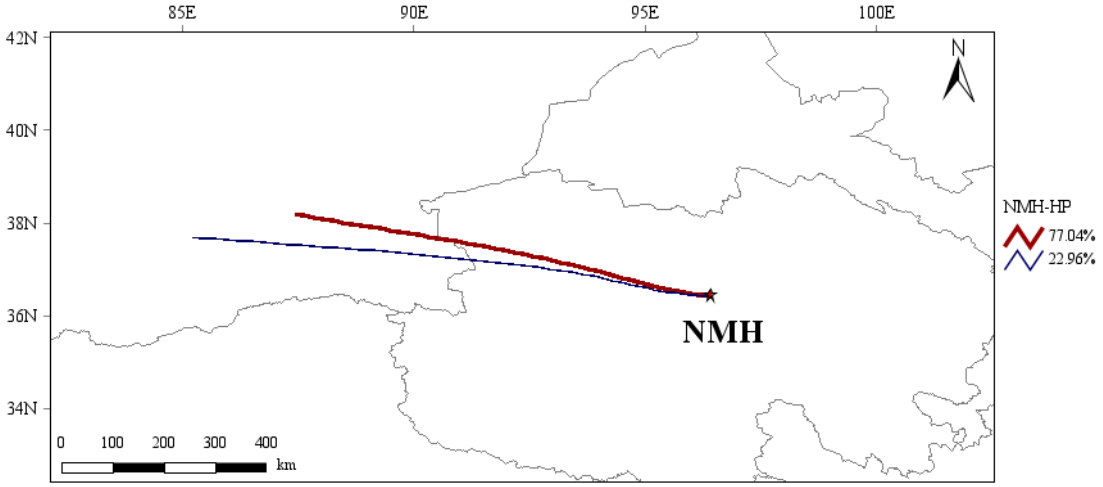
85E
90E
95E
100E
42N
40N
38N
36N
34N
N
NMH-HP
77.04%
22.96%
NMH
0 100 200 300 400
km

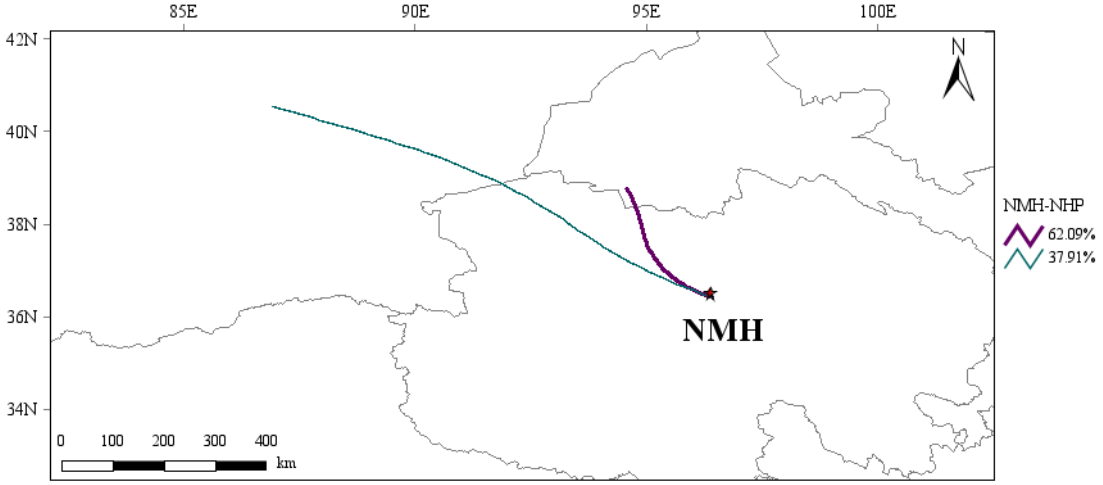
85E
90E
95E
100E
42N
40N
38N
36N
34N
N
NMH-NHP
62.09%
37.91%
NMH
0 100 200 300 400
km

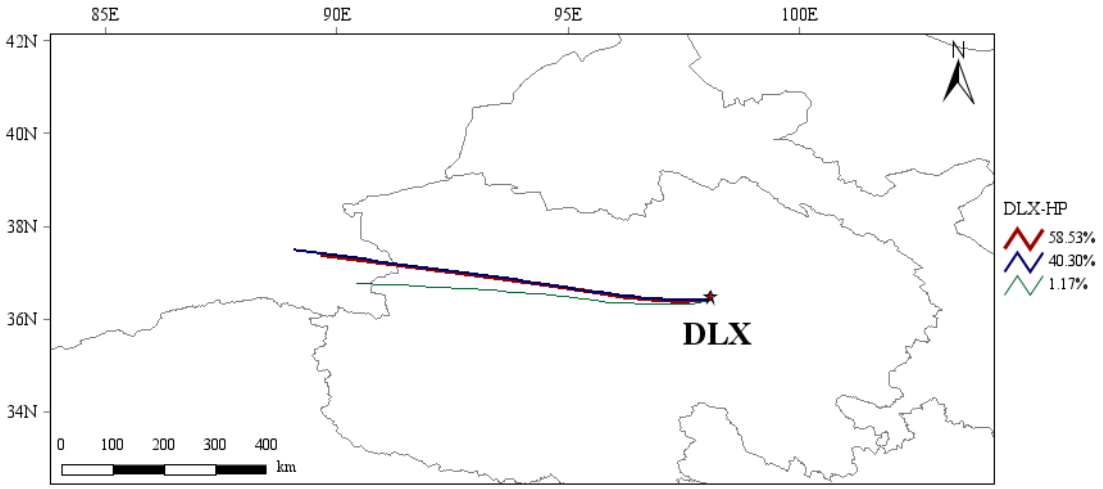
85E
90E
95E
100E
42N
40N
38N
36N
34N
N
DLX-HP
58.53%
40.30%
1.17%
DLX
0 100 200 300 400
km

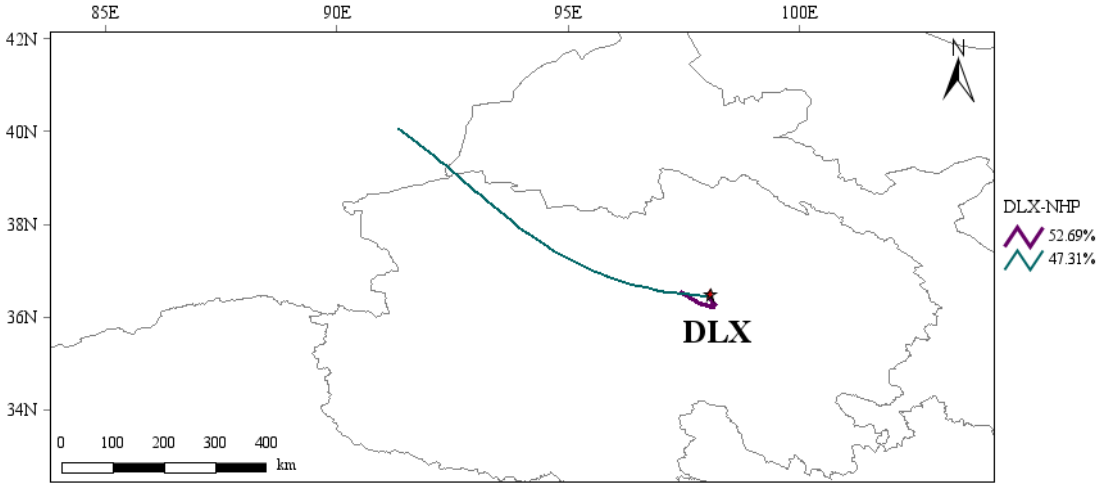

Figure S5 Backward trajectory simulations were conducted at urban monitoring stations during heating and non-heating periods. Different colors denote distinct trajectory paths, while line thickness indicates the degree of contribution from each path. The red star marks the location of the stations. [HP, Heating period; NHP, Non-heating period; GEM, Golmud station; NMH, Nuo Muhong station; DLX, Dulan station].

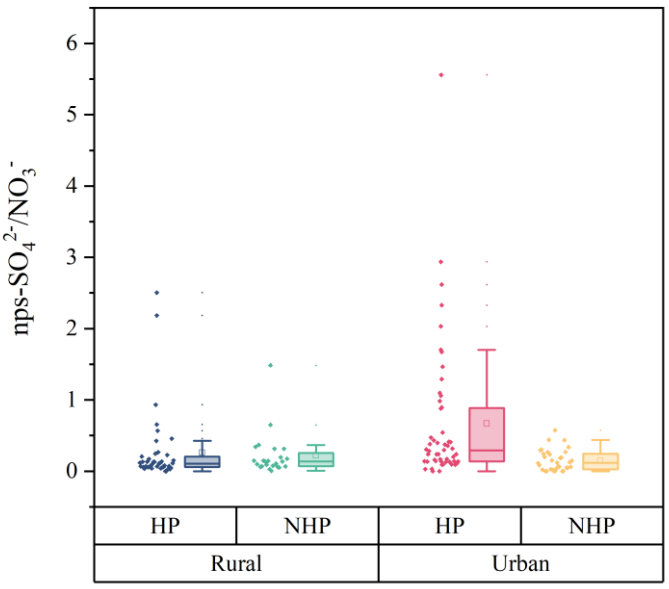

Figure S6 The ratio of nps-SO_4^{2-} to NO_3^- in soluble ions during heating and non-heating periods in rural and urban areas. HP: heating period; NHP: non-heating period.

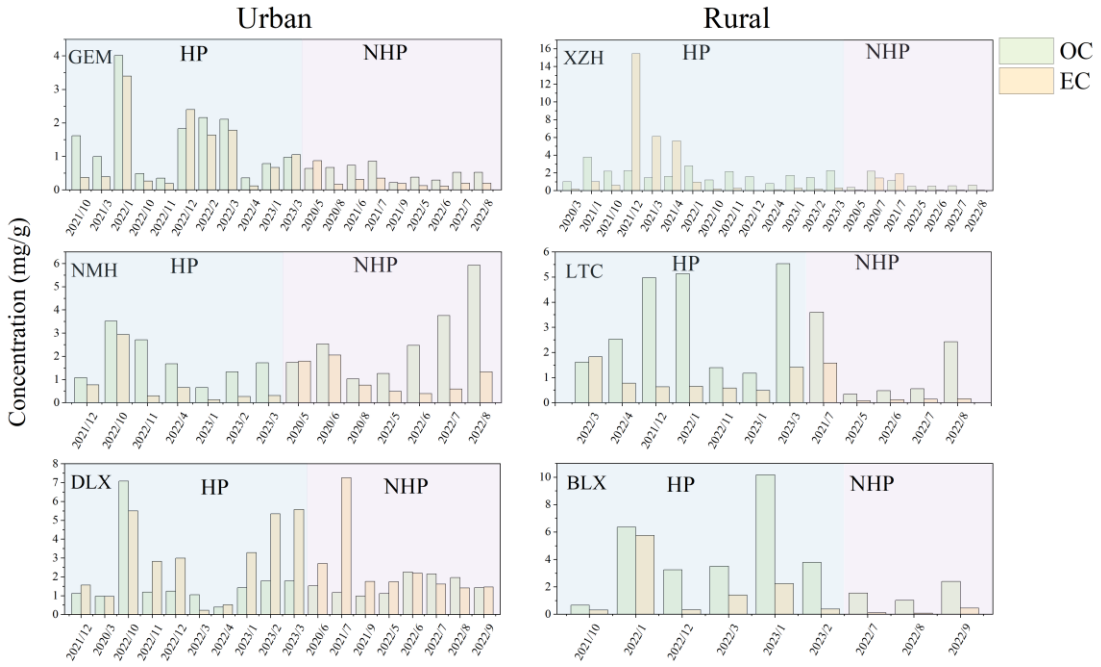

Figure S7 Temporal variations in organic (OC) and element carbon (EC) concentration at six monitoring sites during heating and non-heating periods. HP, Heating period; NHP, Non-heating period; XZH, Xiao Zaohuo station; GEM, Golmud station; LTC, Da Gele station; NMH, Nuo Muhong station; BLX, Balong station; DLX, Dulan station

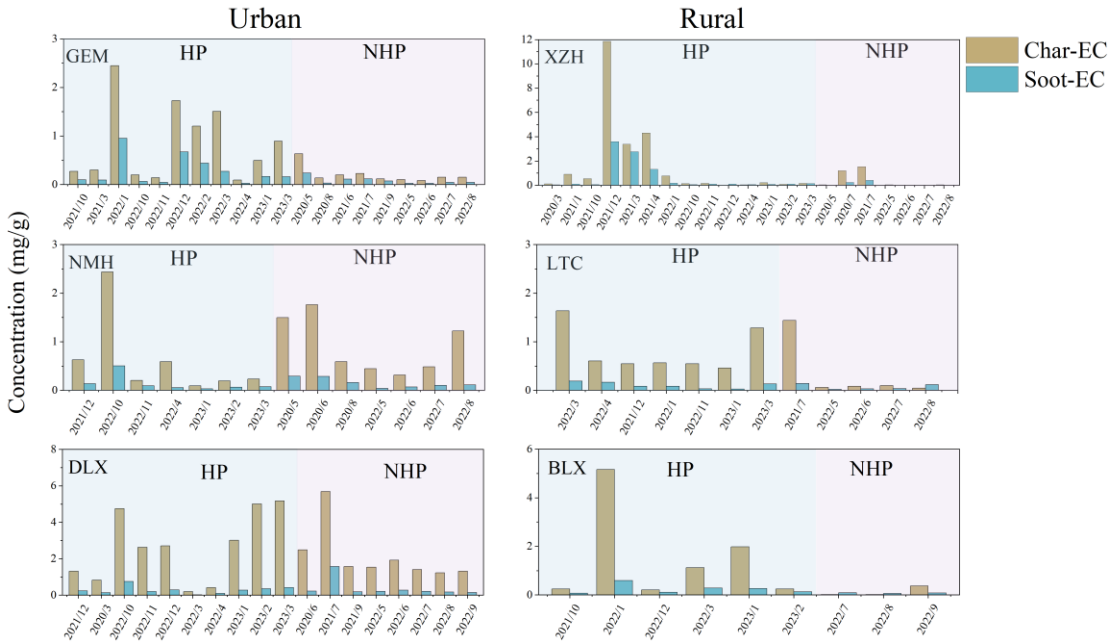

Figure S8 Temporal variations in Char-OC and Soot-EC concentration at six monitoring sites during heating and non-heating periods. HP, Heating period; NHP, Non-heating period; XZH, Xiao Zaohuo station; GEM, Golmud station; LTC, Da Gele station; NMH, Nuo Muhong station; BLX, Balong station; DLX, Dulan station

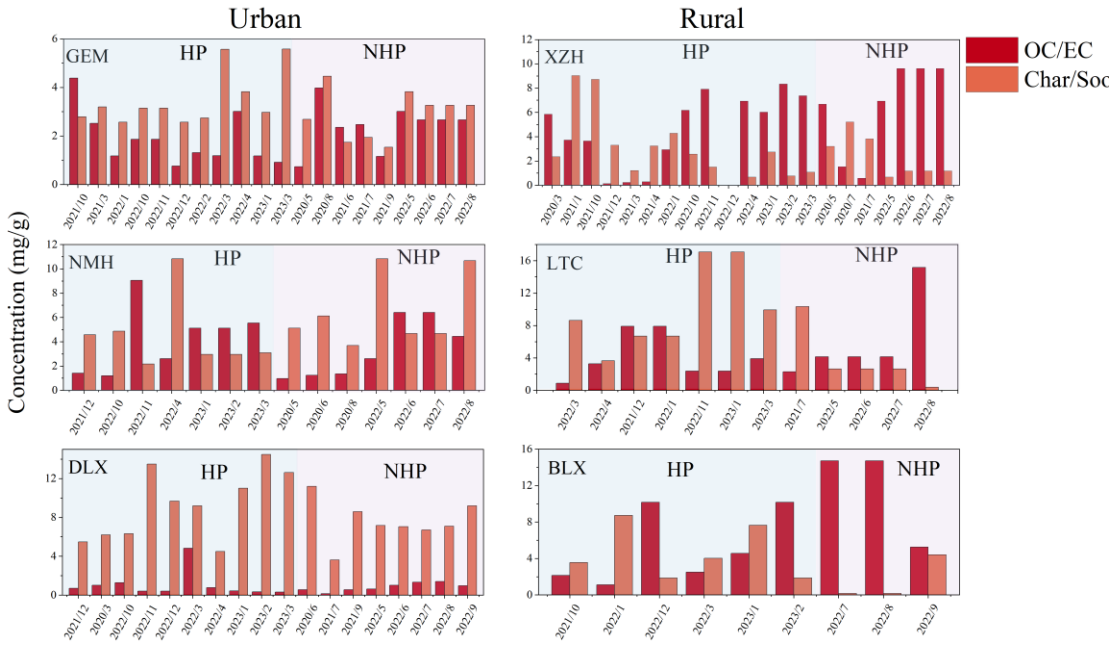

Figure S9 Temporal variations in OC/EC and Char/Soot ratio at six monitoring sites during heating and non-heating periods. HP, Heating period; NHP, Non-heating period; XZH, Xiao Zaohuo station; GEM, Golmud station; LTC, Da Gele station; NMH, Nuo Muhong station; BLX, Balong station; DLX, Dulan station

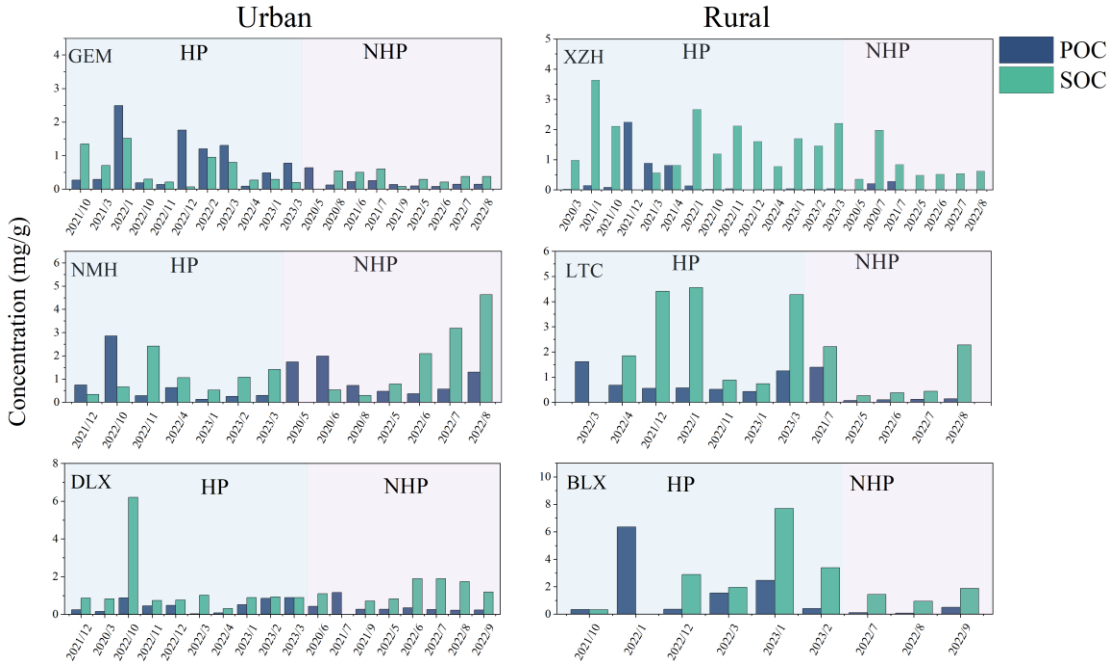

Figure S10 Temporal variations in primary (POC) and secondary organic carbon (SOC) concentration at six monitoring sites during heating and non-heating periods. HP, Heating period; NHP, Non-heating period; XZH, Xiao Zaohuo station; GEM, Golmud station; LTC, Da Gele station; NMH, Nuo Muhong station; BLX, Balong station; DLX, Dulan station

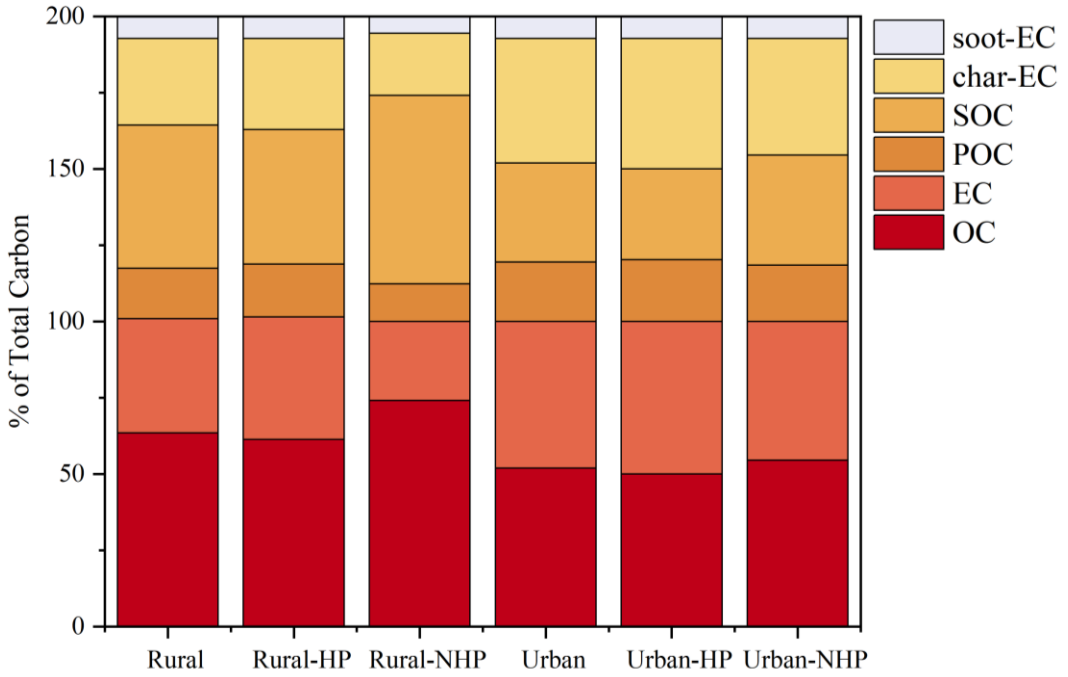

Figure S11 Proportions of various carbon indicators in urban and rural during heating and non-heating periods. HP, Heating period; NHP, Non-heating period.

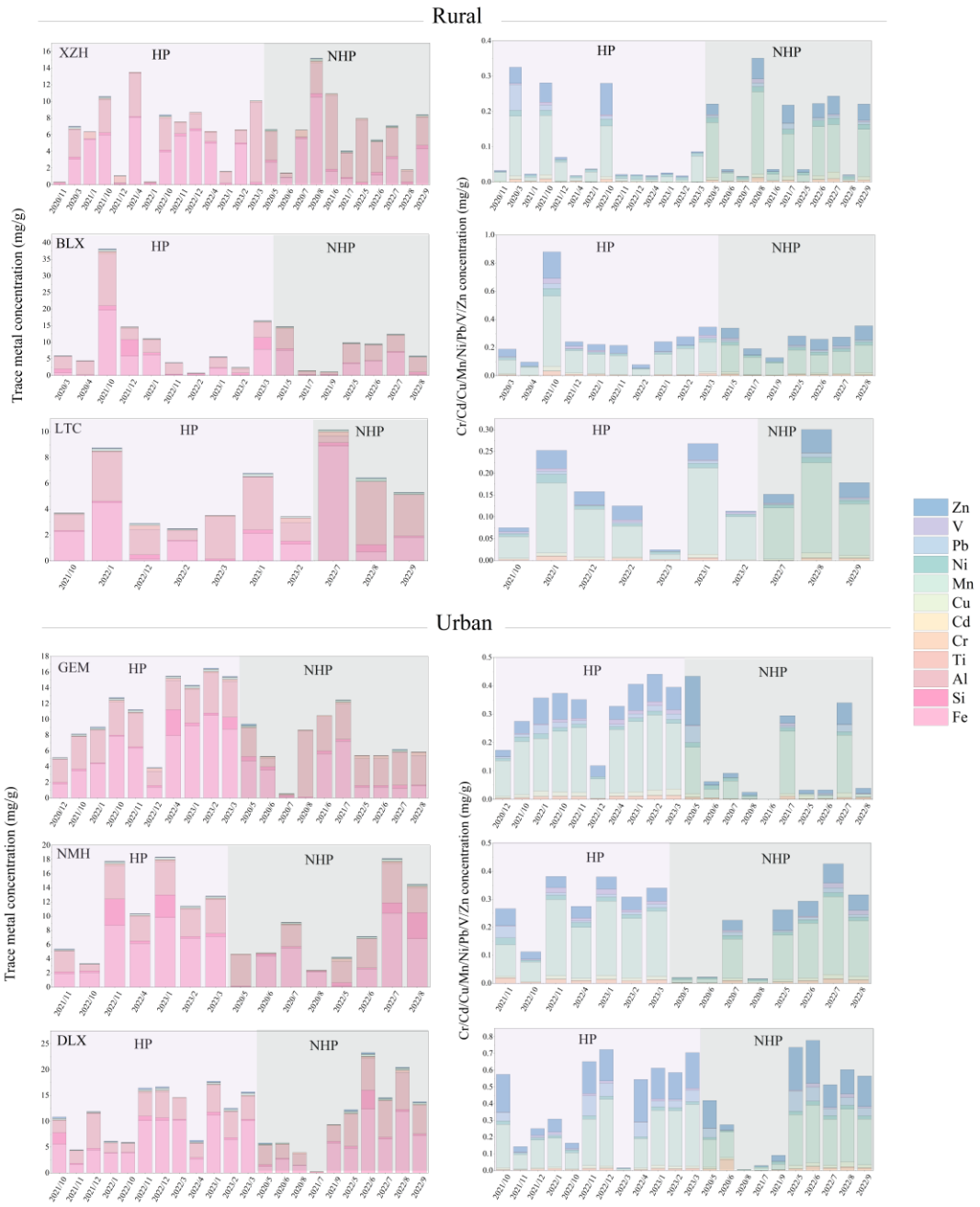

Figure S12 Temporal variations in trace element content at six monitoring sites during heating and non-heating periods. The left panels display trace element concentrations (mg/g) for each site, while the right panels illustrate the smaller concentrations of Cr, Cd, Cu, Mn, Ni, Pb, V, Zn. [HP, Heating period; NHP, Non-heating period; XZH, Xiao Zaohuo station; GEM, Golmud station; LTC, Da Gele station; NMH, Nuo Muhong station; BLX, Balong station; DLX, Dulan station]

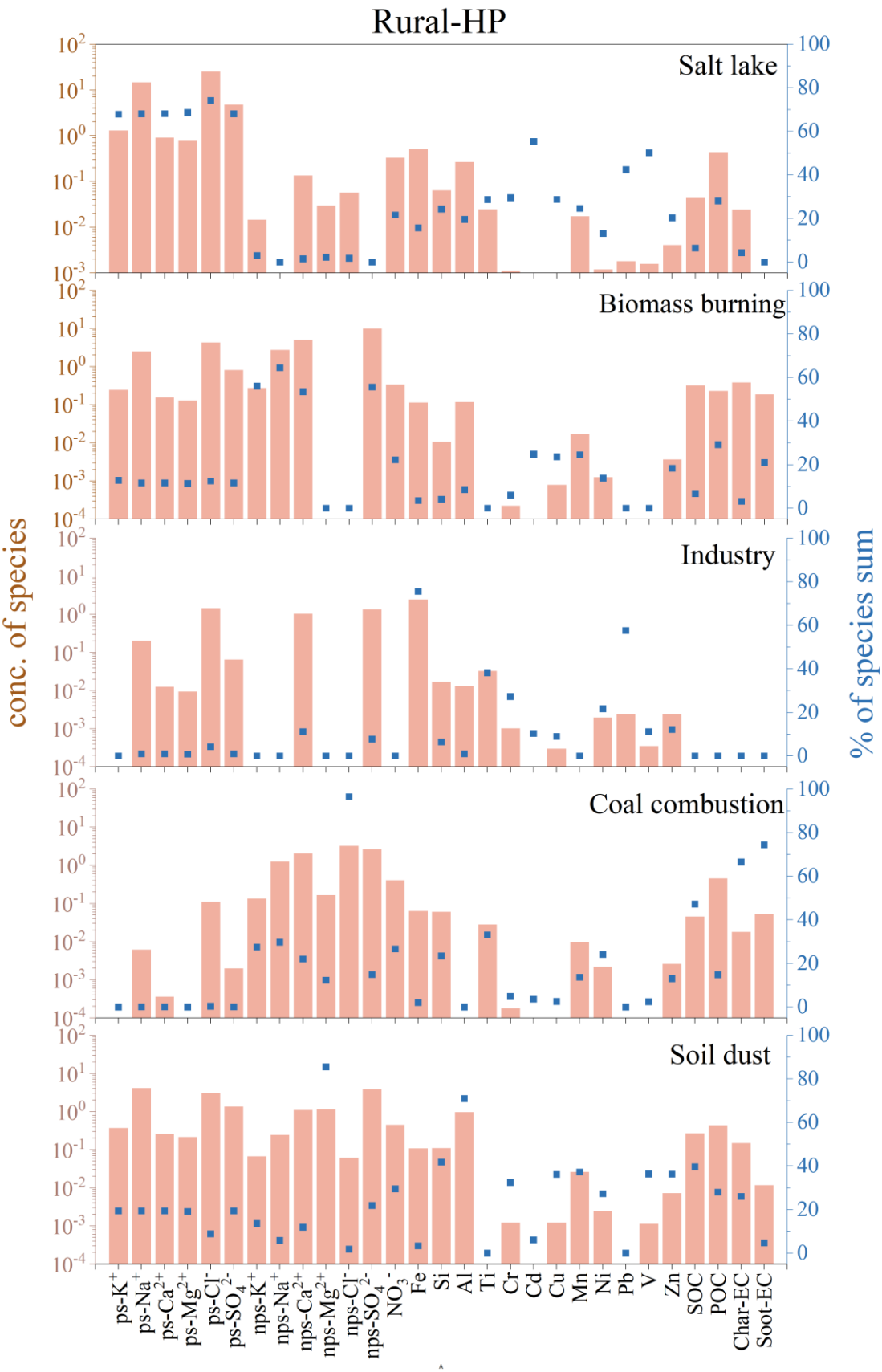
Rural-HP
Salt lake
Biomass burning
Industry
Coal combustion
Soil dust
conc. of species
% of species sum
ps-K+
ps-Na+
ps-Ca2+
ps-Mg2+
ps-Cl-
ps-SO42-
nps-K+
nps-Na+
nps-Ca2+
nps-Mg2+
nps-Cl-
nps-SO42-
NO3-
Fe
Si
Al
Ti
Cr
Cd
Cu
Mn
Ni
Pb
V
Zn
SOC
POC
Char-EC
Soot-EC

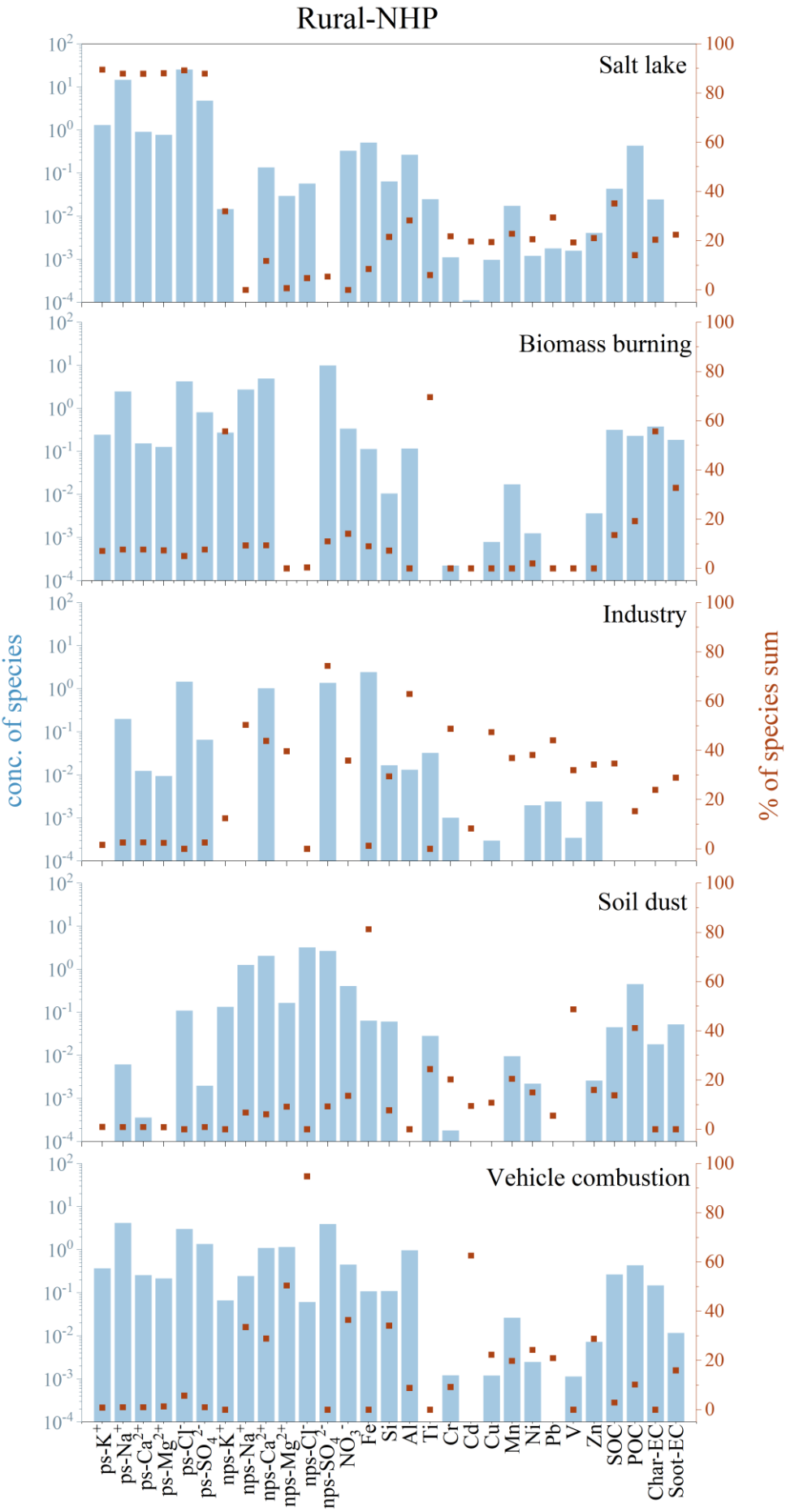
Rural-NHP
Salt lake
Biomass burning
Industry
Soil dust
Vehicle combustion
conc. of species
% of species sum
ps-K+
ps-Na+
ps-Ca2+
ps-Mg2+
ps-Cl-
ps-SO4 2-
nps-K+
nps-Na+
nps-Ca2+
nps-Mg2+
nps-Cl-
nps-SO4 2-
NO3 -
Fe
Si
Al
Ti
Cr
Cd
Cu
Mn
Ni
Pb
V
Zn
SOC
POC
Char-EC
Soot-EC

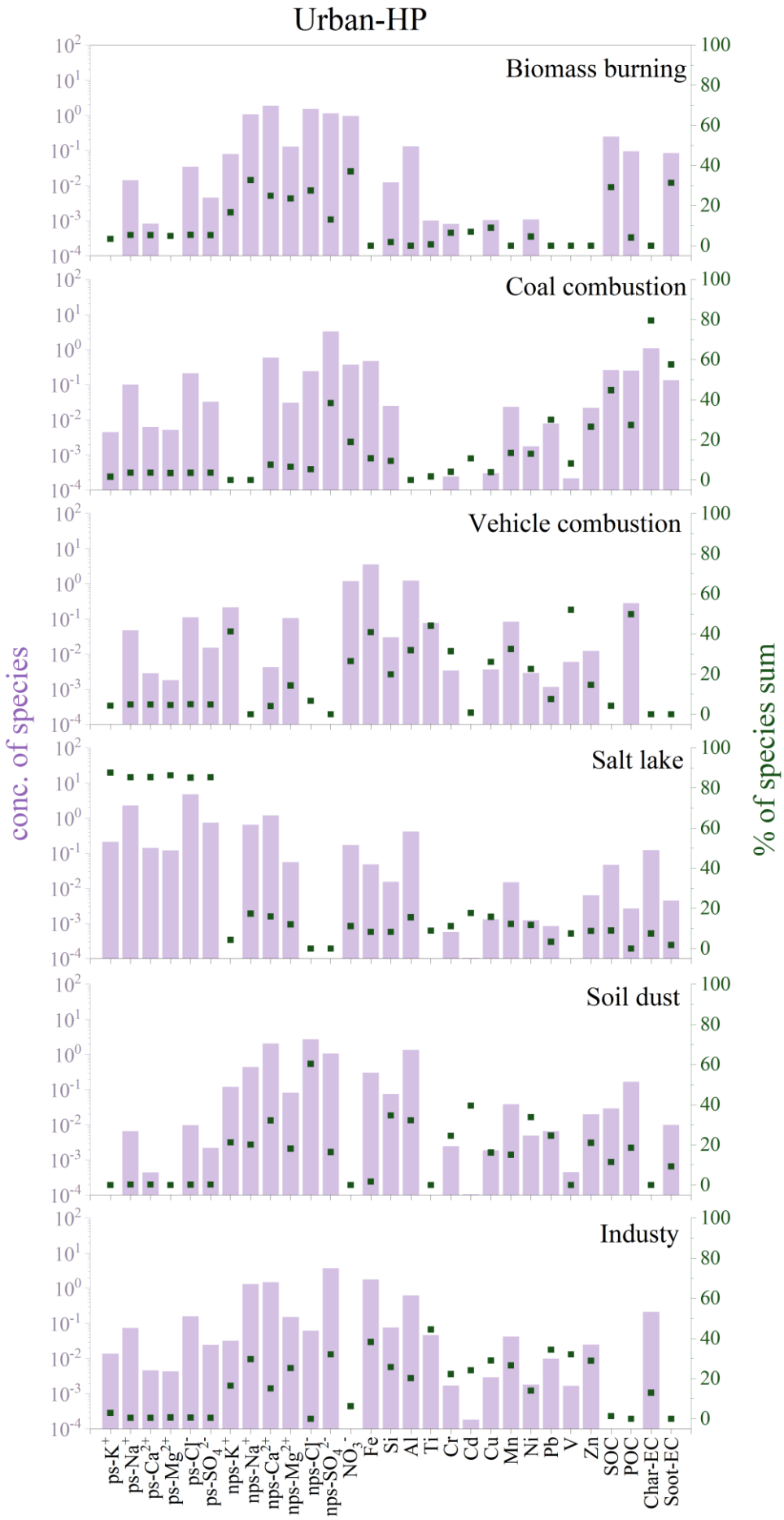
Urban-HP
Biomass burning
Coal combustion
Vehicle combustion
Salt lake
Soil dust
Industy
conc. of species
% of species sum
ps-K+
ps-Na+
ps-Ca2+
ps-Mg2+
ps-Cl-
ps-SO4 2-
nps-K+
nps-Na+
nps-Ca2+
nps-Mg2+
nps-Cl-
nps-SO4 2-
NO3 -
Fe
Si
Al
Ti
Cr
Cd
Cu
Mn
Ni
Pb
V
Zn
SOC
POC
Char-EC
Soot-EC

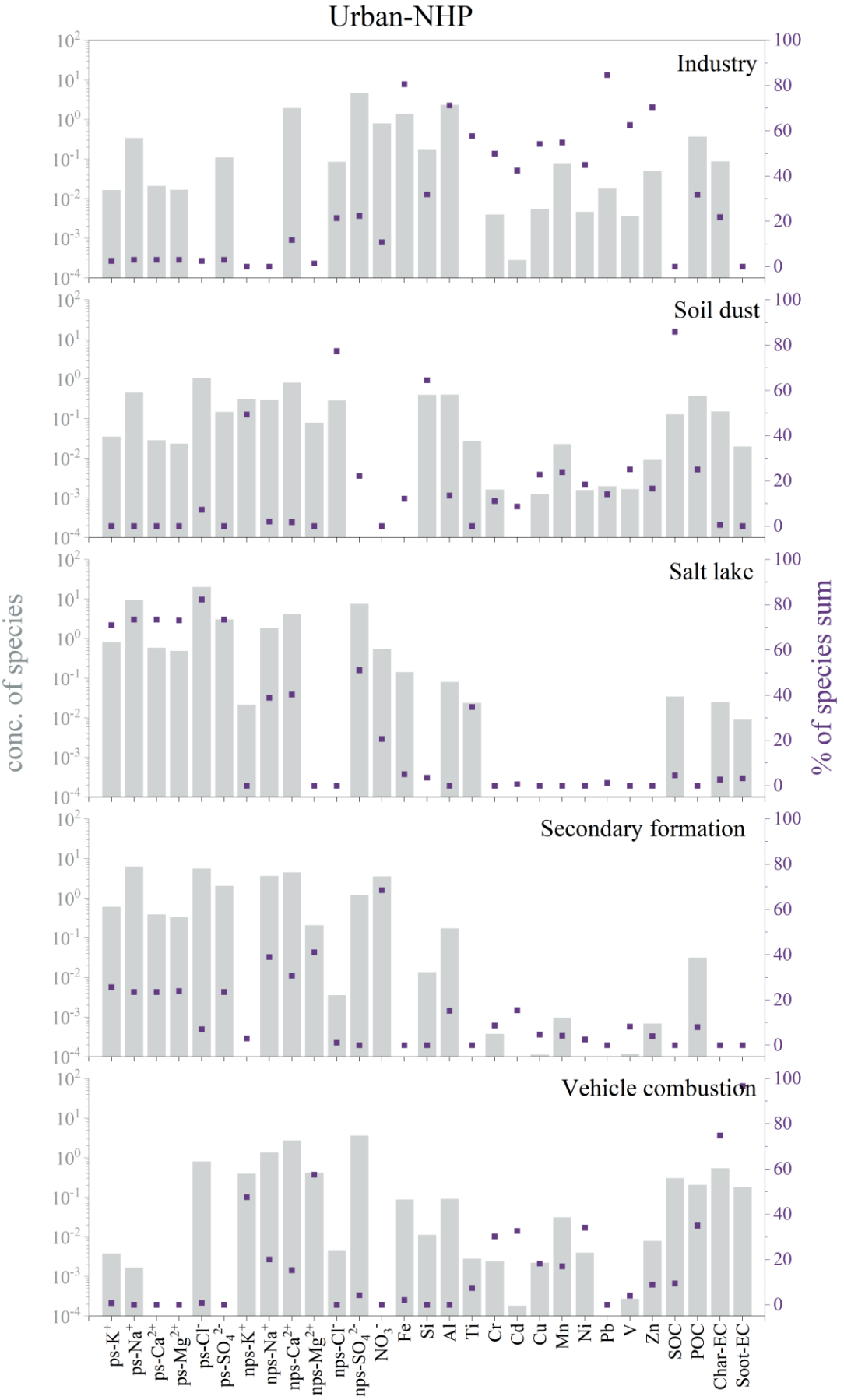
Urban-NHP
Industry
Soil dust
Salt lake
Secondary formation
Vehicle combustion
conc. of species
% of species sum
ps-K+
ps-Na+
ps-Ca2+
ps-Mg2+
ps-Cl-
ps-SO4 2-
nps-K+
nps-Na+
nps-Ca2+
nps-Mg2+
nps-Cl-
nps-SO4 2-
NO3 -
Fe
Si
Al
Ti
Cr
Cd
Cu
Mn
Ni
Pb
V
Zn
SOC
POC
Char-EC
Soot-EC

Figure S13 Species profiles and contributions of each resolved source for rural and urban areas during heating and non-heating periods, as determined through PMF dust-fall source apportionment. Contribution of species are presented in a histogram, while the species profile is depicted in a scatter plot. [HP, heating period; NHP non-heating period].